ENVIRONMENTAL ENGINEERING SCIENCE
Volume 32, Number 3, 2015

DOI: 10.1089/ees.2013.0260

Novel NO_2^- Sensor Using $PW_{12}O_{40}^{3-}$/Chitosan-Graphene Nanocomposites/Cysteamine/Gold Electrode

Xia Li,[1] Changting Wei,[1] Yonghai Song,[1] Haozhi Zhu,[1] Shouhui Chen,[1] Ping Li,[1] Lanlan Sun,[2] and Li Wang[1,*]

[1]*Key Laboratory of Functional Small Organic Molecule, Ministry of Education, College of Chemistry and Chemical Engineering, Jiangxi Normal University, Nanchang, People's Republic of China.*
[2]*State Key Laboratory of Luminescence and Applications, Changchun Institute of Optics, Fine Mechanics and Physics, Chinese Academy of Sciences, Changchun, People's Republic of China.*

Received: July 30, 2013 *Accepted in revised form: November 8, 2014*

Abstract

A novel nitrite (NO_2^-) sensor was fabricated by electrodepositing phosphotungstic acid ($PW_{12}O_{40}^{3-}$) on chitosan (CHIT)-graphene nanocomposites modified cysteamine/gold (Au) electrode. Fourier transform infrared spectroscopy, Raman spectroscopy, X-ray powder diffraction, X-ray photoelectron spectroscopy, scanning electron microscopy, and atomic force microscopy were used to study the CHIT-graphene nanocomposites and the $PW_{12}O_{40}^{3-}$/CHIT-graphene/cysteamine/Au electrode. Cyclic voltammograms and chronoamperometric were used to evaluate electrochemical and electrocatalytic properties of the $PW_{12}O_{40}^{3-}$/CHIT-graphene/cysteamine/Au electrode. Electrochemical results showed that the $PW_{12}O_{40}^{3-}$/CHIT-graphene/cysteamine/Au electrode exhibited good electrochemical behaviors and electrocatalytic performance toward the reduction of NO_2^-. Electrocatalytic performance can be ascribed to large specific surface area and good conductivity of the CHIT-graphene nanocomposites and good electrocatalytic activity of $PW_{12}O_{40}^{3-}$. The sensor showed quick amperometric response, low detection limit, wide linear range, high sensitivity, high stability, and good reproducibility. Analytical performance suggests that it is possible to be a potential candidate for routine NO_2^- analysis.

Key words: electrochemistry; graphene; NO_2^-; $PW_{12}O_{40}^{3-}$; sensor

Introduction

Nitrite (NO_2^-), as an important precursor in the formation of toxic and carcinogenic nitrosoamines, is widely used in food preservative, agricultural fertilizer, and color enhancer. So, increasing attention has been paid to the quantitative determination of NO_2^- and it is imperative to obtain an accurate and efficient method to detect NO_2^- (Bertotti and Pletcher, 1997). Up to now, many techniques including spectrophotometry, chromatography, capillary electrophoresis, and fluorescent spectrometry have been applied in the detection of NO_2^-. However, these methods are apparently expensive or time consuming. Recently, much attention has been focused on electrochemical techniques due to its intrinsic reliability, sensitivity, selectivity, and simplicity (Chen *et al.*, 2008; Liu *et al.*, 2010).

Polyoxometalates (POMs), as a class of structurally well-defined anionic clusters with an enormous disparity in size, composition, and function, attracts much attention. Its inherent metal-oxygen framework can possess reversible and gradual multi-electron reaction. As a result, POM has become an attractive candidate in electrode modification and electrocatalytic research (Chen *et al.*, 2008). Some POM modified electrodes have been constructed for NO_2^- detection in recent years (Rahman *et al.*, 2006; Hamidi *et al.*, 2008; Li *et al.*, 2008; Gu *et al.*, 2009). For example, Indium-Tin Oxide (ITO) electrode modified by one-dimensional POM hybrid nanofibers has been reported by Cao *et al.* (2012), and layer by layer hybridized POM and poly(ferrocenylsilane) on a cysteamine modified gold electrode has been reported by our group (Chen *et al.*, 2008).

Electrodeposition has become a popular method to attach POMs onto the surface of electrodes owing to their properties of quick assembly and simple operation. To obtain a good catalytic activity, the electrodeposition of POMs on cystamine modified gold electrode has been developed (Chen *et al.*, 2009). However, the packed density of POMs was only monolayer on cystamine modified gold electrode surface, which is unfavorable for its electrocatalytic performance. Meanwhile, some conductive polymer (Molina *et al.*, 2008), cysteamine (Chen *et al.*, 2009), poly(ferrocenylsilane) (Chen *et al.*, 2008), and others, have also been used to modify

**Corresponding author:* Key Laboratory of Functional Small Organic Molecule, Ministry of Education, College of Chemistry and Chemical Engineering, Jiangxi Normal University, 99 Ziyang Road, Nanchang 330022, People's Republic of China. *Phone:* 86-791-8120861; *Fax:* 86-791-8120861; *E-mail:* lwang@jxnu.edu.cn

electrode for POMs deposition as sensor for NO_2^- detection. Graphene, a single layer of carbon atoms in a closely packed honeycomb two-dimensional lattice, has attracted tremendous attention because of its excellent electrical properties and the high specific surface area of 400 m^2/g up to 1,500 m^2/g for metal NPs deposition or enzyme adsorption on electrodes (Wang *et al.*, 2010), especially chemically derived graphene by chitosan (CHIT) owing to its abundant groups, such as epoxide, hydroxyl and carboxylic groups, and the high hydrophilcity (Yang *et al.*, 2010). The remarkable surface area and its well electrocatalytic and electrochemical properties have led to an explosion of research in the field of electrochemical sensors.

In this work, $PW_{12}O_{40}^{3-}$ was electrodeposited on an Au electrode that was modified with CHIT-graphene/cysteamine to fabricate a NO_2^- sensor. The CHIT-graphene nanocomposites exhibited high conductivity and large specific surface area, which resulted in a large number of $PW_{12}O_{40}^{3-}$ assembled on electrode surface and improved the electron transfer and electrocatalytic activity of $PW_{12}O_{40}^{3-}$. Cyclic voltammetry and chronoamperometry were used to investigate electrocatalytic behavior of the modified electrode toward NO_2^-. The analytical performance of the sensor related to the sensitivity, detection limit, linear range, response time, selectivity, and stability have been discussed in detail.

Materials and Methods

Reagent

CHIT, $PW_{12}O_{40}^{3-}$ and cysteamine were obtained from Sigma-Aldrich. $NaNO_2$ and other reagents were purchased from Beijing Chemical Reagent Factory. All reagents were of analytical grade and used without further purification. The 1.0 M H_2SO_4 as support electrolyte was purged with high purity nitrogen. All solutions were prepared with ultrapure water, purified by a Millipore–Q system (18.2 MΩ·cm).

Preparation of CHIT-graphene nanocomposites

CHIT-graphene was prepared according to previous reported method (Wang *et al.*, 2012). Briefly, graphene oxide (GO) was first prepared according to the Hummers method (Hummers and Offeman, 1958). Graphite powder was added into 20 mL ultrapure water and ultrasonicated for 45 min to get GO suspension. Then, 5.0 mg of CHIT was dissolved in 1 mL 1% acetic acid to get 0.5 wt% CHIT and the pH was adjusted to 5–6 by adding appropriate NaOH. Then, 10 mL GO suspension (0.1 mg/mL) was mixed with 10 mL 0.5 wt% CHIT solution and was stirred for 24 h at room temperature to obtain the CHIT-GO nanocomposites.

The resulted CHIT-GO nanocomposites were ultrasonicated for 40 min. After 3.5 μL hydrazine hydrate and 40 μL ammonia solution were added, the mixture was kept at 90°C for 1 h. The product was finally dialyzed in dialytic membrane for 24 h. The derived CHIT-graphene nanocomposites were well soluble in water and ethanol.

Preparation of $PW_{12}O_{40}^{3-}$/CHIT-graphene/cysteamine/Au electrode

Au electrode ($\phi = 2$ mm) was polished with 1.0, 0.3, and 0.05 μm Al_2O_3 powders on felt pads to obtain a mirror-like surface before experiments, then ultrasonicated with copious amount of ultrapure water and absolute ethanol for 1 min and dried by N_2. This freshly pretreated Au electrode was immersed in 1.0 mM ethanol solution of cysteamine for 24 h and followed by thoroughly ultrasonicating with absolute ethanol to eliminate physically adsorbed cysteamine. Subsequently, the cysteamine/Au electrode was immersed in CHIT-graphene solution for 12 h to give a CHIT-graphene/cysteamine/Au electrode. Then, the CHIT-graphene/cysteamine/Au electrode was scanned in the potential range from −0.4 to 0.4 V at 100 mV/s for 100 cycles in 1.0 M H_2SO_4 containing 3.0 mM $PW_{12}O_{40}^{3-}$ to produce the $PW_{12}O_{40}^{3-}$/CHIT-graphene/cysteamine/Au electrode. The procedure of the modified electrode was shown in Fig. 1. The prepared modified electrodes were kept at 4°C for future use. As a control, $PW_{12}O_{40}^{3-}$/cysteamine/Au electrode was also made according to above process.

Apparatus

All electrochemical experiments were performed by a CHI 660C electrochemical workstation (CH Instrument). A conventional three-electrode system was used with modified Au electrode as working electrode, a platinum wire as auxiliary electrode, and a saturated calomel electrode as reference electrode. The cyclic voltammetric experiments were performed in a quiescent solution. The amperometric experiments were carried out under a continuous stirring using a magnetic stirrer. About 1.0 M H_2SO_4 was used as the supporting electrolyte solution, purged with high purity N_2 for 30 min before measurements and then a N_2 atmosphere was kept over the solution during measurements.

Atomic force microscopy (AFM) measurements were carried out with an AJ-III (Shanghai Aijian Nanotechnology) in tapping mode. Standard silicon cantilevers (spring constant,

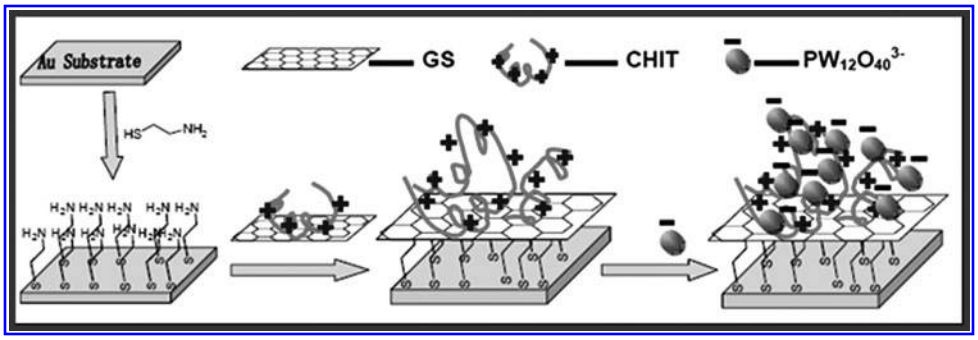

FIG. 1. Schematic representation of procedure for the electrode construction.

0.6–6 N/m) were used under its resonance frequency (typically, 60–150 kHz) at room temperature under ambient condition. Fourier transform infrared spectroscopy (FTIR) was obtained on a Perkin-Elmer Spectrome 100 spectrometer (Perkin-Elmer Company). Raman spectra were collected using a Renishaw 2000 model confocal microscopy Raman spectrometer with a CCDS detector and a holographic notch filter (Renishaw Ltd.). Scanning electron microscopy (SEM) analysis was taken using a XL30 ESEM-FEG SEM at an accelerating voltage of 20 kV equipped with a Phoenix energy dispersive X-ray analyzer. X-ray powder diffraction (XRD) data were collected on a D/Max 2500V/PC X-ray powder diffractometer using Cu Kα radiation ($\lambda = 1.54056$ Å, 40 kV, 200 mA).

Results and Discussion

Characteristics of sensor

FTIR was first employed to study the CHIT-graphene nanocomposites (Fig. 2A). For graphene, there were only two vibration peaks at 1,579 and 1,248 cm^{-1} belonging to C = C and C-C, respectively (Yang *et al.*, 2010). For CHIT-graphene nanocomposites, two characteristic absorbance bands centered at 1,642 and 1,567 cm^{-1}, which corresponded to the C = O stretching vibration of -NHCO- and the N-H bending of $-NH_2$, respectively, indicating CHIT has been successfully assembled on graphene surface.

Additional information on the structure of the materials was provided by Raman spectroscopy. In Fig. 2B, two bands were observed on the spectrum of the CHIT-graphene nanocomposites at 1,348 cm^{-1} (D band) and 1,595 cm^{-1} (G band), respectively. The D band came from carbon with sp^3 hybridization, corresponding to disordered and defective carbon atoms, while the G band was the results of in-phase vibration of the graphene lattice, indicating ordered region in the graphene lattice. The intensity ratio of D and G band (I_D/I_G) could be used to quantify the relative content of defects and the sp^2 domain. After the hydrazine reduction, the I_D/I_G of graphene should increase according to previous results (Han *et al.*, 2010). After the CHIT-GO was reduced to CHIT-graphene, the two bands became narrow and the I_D/I_G increased, indicating higher degree of disorder (Stankovich *et al.*, 2007). The result confirmed that the CHIT-GO was successfully reduced into CHIT-graphene. As shown in Fig. 2B, both the characteristics peaks of CHIT-graphene (1,348 and 1,595 cm^{-1}) and $PW_{12}O_{40}^{3-}$ (974 and 993 cm^{-1}) were simultaneously observed on the Raman spectrum of the $PW_{12}O_{40}^{3-}$/CHIT-graphene nanocomposites. The result confirmed that the nanocomposites consisted of CHIT-graphene and $PW_{12}O_{40}^{3-}$.

XRD patterns were measured to examine the crystal structures of CHIT-graphene and solid product of deposition. As shown in Fig. 2C, a broad peak, which was the characteristic of amorphous material, was observed, indicating that the CHIT-graphene was amorphous material. After deposition of $PW_{12}O_{40}^{3-}$, the diffraction peaks matched well with the reported $PW_{12}O_{40}^{3-}$ (Zhu *et al.*, 2013). From those XRD results, it could be concluded that the crystalline $PW_{12}O_{40}^{3-}$ was electrodeposited on the amorphous CHIT-graphene successfully.

Morphology of as-prepared graphene and CHIT-graphene nanocomposites were characterized by AFM (Fig. 3). Individual graphene sheets could be easily observed on mica surface (Fig. 3A). The graphene has lateral dimensions from several micrometers with a thickness of 0.8 nm as shown by its section analysis (Fig. 3A), which was characteristic of fully exfoliated graphene sheets. The AFM image of CHIT-graphene nanocomposites showed a very rough surface (Fig. 3B), suggesting CHIT and graphene formed CHIT-graphene nanocomposites. The thickness of CHIT-graphene sheet measured by section analysis was about 2.0 nm (Fig. 3B). Since the size of the CHIT was about 0.5 nm and the thickness of the graphene was about 1.0 nm, it was reasonable to conclude that the CHIT-graphene nanocomposites consisted of one layer of graphene and mono- or submonolayer of CHIT on both of its surfaces.

SEM images revealed the surface morphology of the modified electrode and were shown in Fig. 4. It clearly showed that a large number of CHIT-graphene nanocomposites with wrinkled structure were assembled on cysteamine/Au electrode (Fig. 4A, B). After the $PW_{12}O_{40}^{3-}$ was electrodeposited on CHIT-graphene/cysteamine/Au electrode, the crystals $PW_{12}O_{40}^{3-}$ closely wrapped by wrinkled and thin layer of CHIT-graphene were tightly fixed on the electrode (Fig. 4C, D). The graphene layer might act as conducting medium to accelerate the electrons transfer among the analytes, the $PW_{12}O_{40}^{3-}$ catalyst, and the electrode.

Direct electrochemical properties of $PW_{12}O_{40}^{3-}$/CHIT-graphene/cysteamine/Au electrode

Cyclic voltammetry was used to investigate direct electrochemical behaviors of $PW_{12}O_{40}^{3-}$/CHIT-graphene/cysteamine/Au electrode. Figure 5A presented cyclic

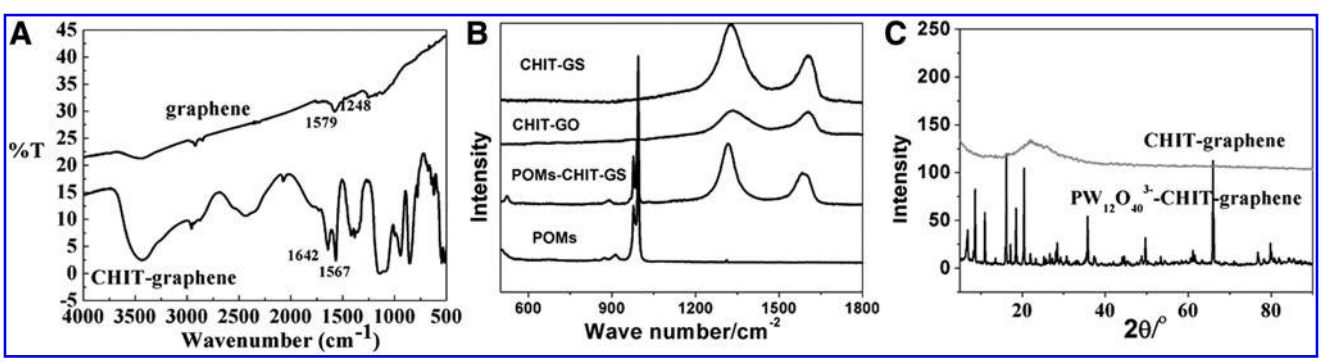

FIG. 2. **(A)** Fourier transform infrared spectroscopy spectra of graphene and chitosan (CHIT)-graphene. **(B)** Raman spectra of CHIT-graphene oxide, CHIT-graphene, $PW_{12}O_{40}^{3-}$/CHIT-graphene, and $PW_{12}O_{40}^{3-}$. **(C)** X-ray powder diffraction pattern of CHIT-graphene and $PW_{12}O_{40}^{3-}$/CHIT-graphene.

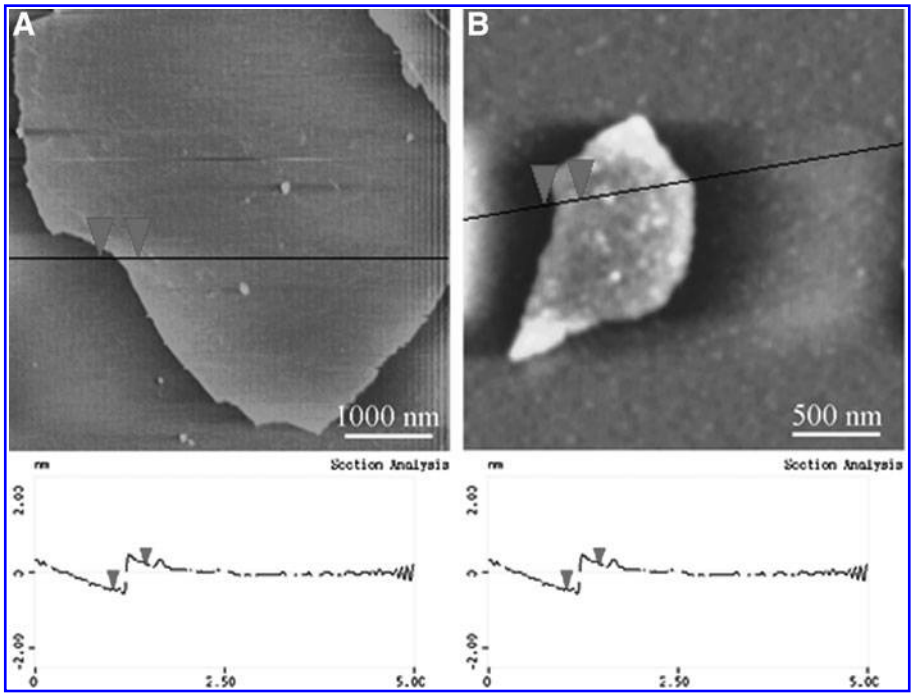

FIG. 3. Atomic force microscopy images and their corresponding section analysis of graphene **(A)** and CHIT-graphene **(B)**. The arrowheads indicate the mica surface and graphene or CHITI-graphene surface, respectively.

voltammograms (CVs) curves of different modified electrodes in N_2-satruated 1.0 M H_2SO_4. Both cysteamine/Au electrode (curve a) and CHIT-graphene/cysteamine/Au electrode (curve b) did not show redox peak. After $PW_{12}O_{40}^{3-}$ was electrodeposited on the CHIT-graphene/cysteamine/Au electrode, a reversible redox peak ($E_{pa} = -0.051$ V and $E_{pc} = -1.08$ V) appeared (curve d), which could be attributed to oxidization and reduction of $PW_{12}O_{40}^{3-}$. Noticeably, $PW_{12}O_{40}^{3-}$ in 1.0 M H_2SO_4 usually showed three classical redox peaks appear at near -0.05, -0.35, and -0.65 V. However, the latter two peaks (-0.35 and -0.65 V) were beyond the working voltage (-0.3 to 0.4 V) in the present work. Therefore, only one redox peak at about -0.05 V was observed (Ojani *et al.*, 2008). The electron transfer number was estimated to be 1 according to the peak-to-peak separation (ΔEp) of 57 mV. In comparison with $PW_{12}O_{40}^{3-}$/cysteamine/Au electrode (curve c), the $PW_{12}O_{40}^{3-}$/CHIT-graphene/cysteamine/Au electrode showed a much higher peak current, indicating CHIT-graphene did result in a large number of $PW_{12}O_{40}^{3-}$ assembled on electrode surface owing to its large specific surface area.

The stability of electrode was very important for its actual application. As shown in Fig. 5B, only 3.2% of peak current signal decreased while peak potential remained unchanged

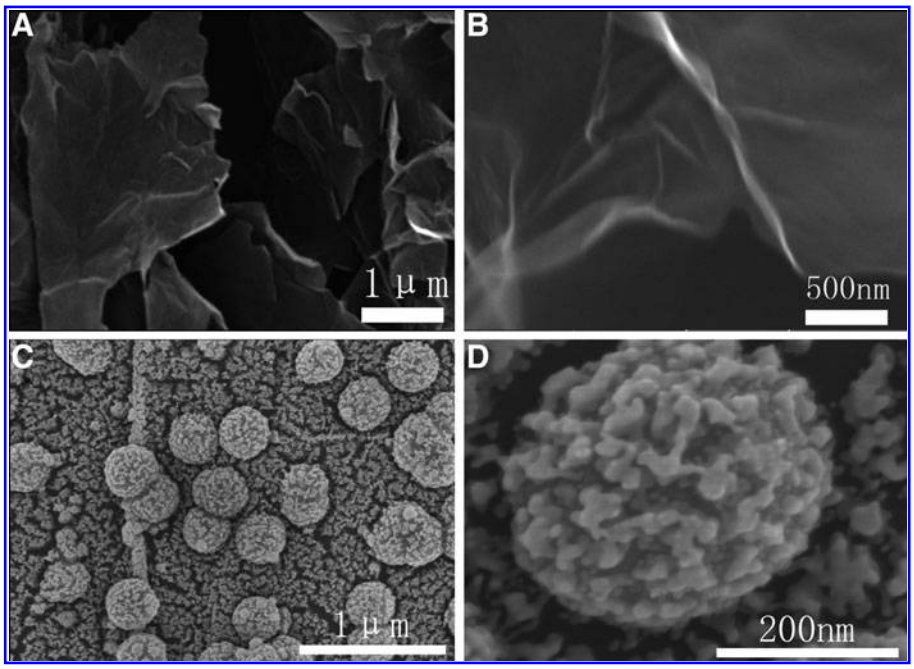

FIG. 4. Scanning electron microscopy images of CHIT-graphene/cysteamine/Au electrode **(A, B)** and $PW_{12}O_{40}^{3-}$/CHIT-graphene/cysteamine/Au electrode **(C, D)**.

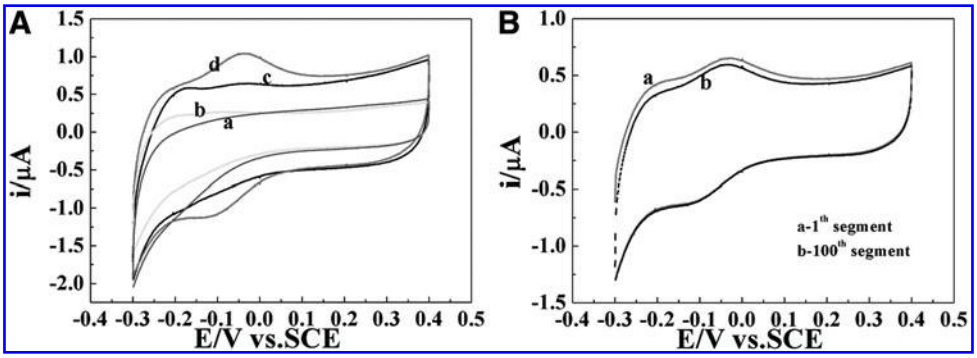

FIG. 5. **(A)** Cyclic voltammograms (CVs) of various electrodes in 1.0 M H_2SO_4: cysteamine/Au electrode (a), CHIT-graphene/cysteamine/Au electrode (b), $PW_{12}O_{40}^{3-}$/cysteamine/Au electrode (c), and $PW_{12}O_{40}^{3-}$/CHIT-graphene/cysteamine/Au electrode (d). **(B)** CVs of $PW_{12}O_{40}^{3-}$/CHIT-graphene/cysteamine/Au electrode in 1.0 M H_2SO_4 with first and 100th scan. Scan rate: 50 mV/s.

after the $PW_{12}O_{40}^{3-}$/CHIT-graphene/cysteamine/Au electrode was scanned for 100 cycles, indicating good stability of the modified electrode.

Figure 6A showed CVs of $PW_{12}O_{40}^{3-}$/CHIT-graphene/cysteamine/Au electrode at different scan rates in 1.0 M H_2SO_4. The peak current was proportionally enhanced with a good linear relation: i_{pa} (nA) = 6.97 + 1.45 υ (V/s) (R = 0.999) for anode peak and i_{pc} (nA) = −84.04–3.07 υ (V/s) (R = −0.997) for cathodic peak (Fig. 6B). The result indicated that the electron transfer reaction involved with a surface-confined process in the studied potential range.

The relationship between peak potential and the logarithm of scan rate was also investigated as shown in Fig. 6C. The anode peak potential shifted positively and the cathodic peak potential shifted negatively as the scan rate increased. E_p was proportional to the logarithm of scan rate from 300 to 900 mV/s as shown in Fig. 6D. The electron transfer coefficient (α) and the rate constant of electrode reaction (k_s) were calculated based on Laviron's theory (Laviron, 1979):

$$E_{pc} = E^{o\prime} + \frac{RT}{\alpha_s nF} - \frac{RT}{\alpha_s nF}\ln v \quad (1)$$

$$E_{pa} = E^{o\prime} + \frac{RT}{(1-\alpha_s)nF} + \frac{RT}{(1-\alpha_s)nF}\ln v \quad (2)$$

where n is the number of electron transfer, R is gas constant (R = 8.314 J/[mol·K]), K is Kelvin temperature (T = 298 K), F is Faraday's constant (F = 96493 C/mol). According to the slopes of the fitting curves, $-2.3RT/\alpha nF$ for cathodic and $2.3RT/(1-\alpha)nF$ for anodic peaks, α was calculated to be 0.41 and n was calculated to be 1. Then, on the basis of the following equation

$$k_s = \alpha nFv/RT \quad (3)$$

the k_s of $PW_{12}O_{40}^{3-}$/CHIT-graphene/cysteamine/Au electrode was calculated to be 2.23 s^{-1} at 100 mV/s.

The effective surface area of the modified electrode was calculated according to the Randles-Sevcik equation;

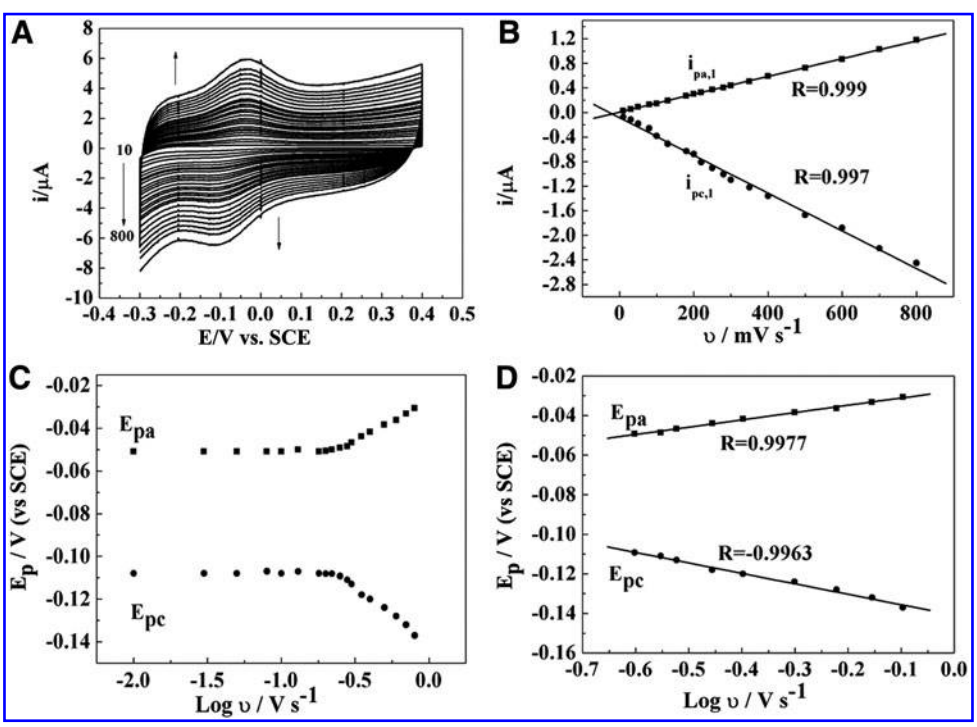

FIG. 6. **(A)** CVs of $PW_{12}O_{40}^{3-}$/CHIT-graphene/cysteamine/Au electrode in 1.0 M H_2SO_4 at various scan rates: 10, 30, 50, 80, 130, 180, 240, 300, 350, 400, 450, 500, 550, 600, 650, 700, and 800 mV/s. The upward and downward arrows indicate the increase and decrease of oxidation peak and reduction peak, respectively. **(B)** Plot of peak current versus scan rate. **(C)** Scatter diagram of peak potential versus scan rate. **(D)** Linear graph of peak potential versus scan rate.

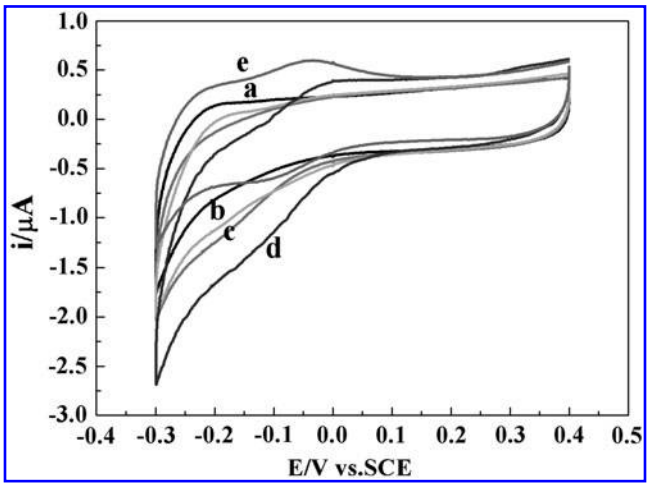

FIG. 7. CVs of various electrodes in 1.0 M H_2SO_4 in the presence (a, b, c, and d) and absence (e) of 0.1 mM NO_2^- at scan rate of 50 mV/s: cysteamine/Au electrode (a), CHIT-graphene/cysteamine/Au electrode (b), $PW_{12}O_{40}^{3-}$/cysteamine/Au electrode (c), and $PW_{12}O_{40}^{3-}$/CHIT-graphene/cysteamine/Au electrode (d, e).

$$I_p = 2.69\times10^{-5} A n^{3/2} D_o^{1/2}\ v^{1/2} C_o^{1/2} \quad (4)$$

where A is effective area, D_o is diffusion coefficient of $K_3Fe(CN)_6$ in 0.1 M KCl ($D_o = 0.673\times10^{-5}$ cm^2/s), υ is the scan rate ($\upsilon = 100$ mV/s), C_o is the concentration of $K_3Fe(CN)_6$ ($C_o = 5$ mM), other symbols have their conventional meanings. The effective surface area of $PW_{12}O_{40}^{3-}$/graphene/cysteamine/Au electrode was 1.07×10^{-4}/cm^2. Surface coverage was also calculated according to Faraday Law (Xu *et al.*, 2010):

$$\Gamma* = \frac{Q}{nFA} \quad (5)$$

where $\Gamma*$ is surface coverage and other symbols have their conventional meanings. The surface coverage of $PW_{12}O_{40}^{3-}$ on CHIT-graphene/cysteamine/Au electrode was estimated to be 1.966×10^{-8} mol/cm^2.

Electrocatalytic activity of $PW_{12}O_{40}^{3-}$/CHIT-graphene/cysteamine/Au electrode toward NO_2^-

Electrocatalytic performance of $PW_{12}O_{40}^{3-}$/CHIT-graphene/cysteamine/Au electrode toward the reduction of NO_2^- was investigated. Figure 7 showed CVs of the various modified electrodes in 1.0 M H_2SO_4 in the presence (curve a, b, c, and d) and absence (curve e) of 0.1 mM NO_2^-. As shown in Fig. 7, no obvious reduction current was observed on cysteamine/Au electrode (curve a) and CHIT-graphene/cysteamine/Au electrode (curve b) in 1.0 M H_2SO_4 in the presence of 0.1 mM NO_2^-. After $PW_{12}O_{40}^{3-}$ was electrodeposited on the CHIT-graphene/cysteamine/Au electrode, an obvious reduction current appeared in curve d, which indicated that the reduction current originated from the reduction of NO_2^- catalyzed by $PW_{12}O_{40}^{3-}$. In comparison with $PW_{12}O_{40}^{3-}$/cysteamine/Au electrode (curve c), the $PW_{12}O_{40}^{3-}$/CHIT-graphene/cysteamine/Au electrode showed a much higher current, indicating that CHIT-graphene did enhance the electrocatalytic performance of $PW_{12}O_{40}^{3-}$ toward the reduction of NO_2^- due to its high conductivity and large specific surface area. The possible reaction mechanism of electrocatalytic reduction of NO_2^- catalyzed by $PW_{12}O_{40}^{3-}$ followed:

$$PW_{12}O_{40}^{3-} + e^- \rightarrow PW_{12}O_{40}^{4-} \quad (6)$$

$$PW_{12}O_{40}^{4-} + HNO_2 \rightarrow PW_{12}O_{40}^{3-} + NO + H_3O^+ \quad (7)$$

Figure 8A showed CVs of $PW_{12}O_{40}^{3-}$/CHIT-graphene/cysteamine/Au electrode in 1.0 M H_2SO_4 with different NO_2^- concentrations. The current response was enhanced with increasing NO_2^- concentration. The linear relationship between current response and NO_2^- concentration was studied by successively adding NO_2^- into 1.0 M H_2SO_4 at −0.18 V. It was obvious that reduction current achieved 95% of the steady-state current in 5 s. Calibration curve of the sensor was also exhibited in Fig. 8B (Inset). The reduction current was proportional to the concentration of NO_2^- in the range of 0.18 μM–6.74 mM ($R = 0.999$). The detection limit was estimated to be 0.06 μM based on the reported equation (Castillo and Castells, 2001):

$$L_D = 3.29(\sigma_{b1}/b_1) \quad (8)$$

where L_D is detection limit, σ_{b1} is deviation based on the response dispersion at blank level ($\sigma_{b1} = 1.95\times10^{-4}$) and b_1 is the slope of the calibration line ($b_1 = 10.55$).

Recently, many NO_2^- sensors have been developed by using POM or other materials. A comparison of the performance of our newly designed sensor with those already

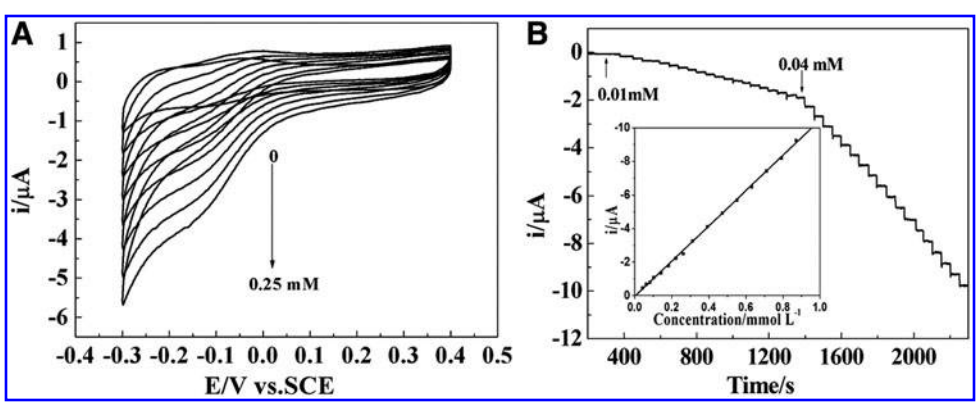

FIG. 8. **(A)** CVs of the $PW_{12}O_{40}^{3-}$/CHIT-graphene/cysteamine/Au electrode in 1.0 M H_2SO_4 in the presence of NO_2^-: concentration range from 0 to 0.25 mM. **(B)** Amperometric responses in a continuous stirring 1.0 M H_2SO_4 at −0.18 V with an increasing NO_2^- concentration for the $PW_{12}O_{40}^{3-}$/CHIT-graphene/cysteamine/Au electrode. *Inset* is the calibration curve of the sensor.

Table 1. Comparison of Performance of $PW_{12}O_{40}^{3-}$/CHIT-Graphene/Cysteamine/Au Electrode with Other NO_2^- Sensors

Electrode	*Detection potential V (vs. SCE)*	k_s s^{-1}	*Detection limit μmol/L*	*Linear rang mmol/L*	*Reference*
$PW_{12}O_{40}^{3-}$/CHIT-graphene/ cysteamine/Au electrode	−0.18	2.23	0.02	0.00018–6.74	This work
$K_6[P_2W_{18}O_{62}]$/ITO electrode	−0.22	—	0.96	0.1–1.5	Cao *et al.* (2012)
Au nanoparticles/ethylenediamine/GCE	−0.6	—	45	0.13–44	Liu and Gu (2008)
POMs(PFS-POMs)$_4$/Cysteamine/ Au electrode	−0.07	—	1.56	0.02–20.36	Chen *et al.* (2008)
PDPA-Pt/GCE	0.86	—	1	0.002–9.5	Unnikrishnan *et al.* (2013)
(CoTsPc PDDA-Gr)$_n$/GCE	0.8	—	0.084	0.002–0.036	Cui *et al.* (2013)
CR-GO/GRE	0.82	—	1	0.0089–0.167	Mani *et al.* (2012)

CHIT, chitosan; GCE, glassy carbon electrode; SCE, saturated calomel electrode.

reported in literature regarding the performance of the NO_2^- assay was listed in Table 1. Taking POMs(PFS-POMs)$_4$/cysteamine/Au electrode as an example, the linear range was fairly wide, but the detection limit was not low enough. Compared with those sensors, the catalytic rate constant, linear response range, sensitivity, and detection limit for NO_2^- detection of the as-prepared sensor in this work were much better. The good catalytic activity and sensitivity might be ascribed to CHIT-graphene nanocomposites, which provided a large specific surface area to increase the quantity of $PW_{12}O_{40}^{3-}$ on electrode surface, improved the conductivity of $PW_{12}O_{40}^{3-}$, and produced a synergistic effect between $PW_{12}O_{40}^{3-}$ and CHIT-graphene.

Interference study

Interference is inevitable in the determination of NO_2^-. Some ions such as Na^+, K^+, Cl^-, and SO_4^{2-} in a five-fold concentration did not show obvious interference to NO_2^- detection, while ClO_3^-, BrO_3^-, IO_3^-, SO_3^{2-}, Fe^{3+}, and ascorbic acid in a two-fold concentration interfered significantly. The repeatability of the current response of one resulted sensor to five successive amperometric measurements of 0.5 mM NO_2^- was checked. A relative standard deviation value (RSD) of 3.26% was calculated for the steady current density. The reproducibility was determined from the response to 0.5 mM NO_2^- at five different sensors. They yielded a RSD of 4.56%. When the electrode was stored in 1.0 M H_2SO_4 for 2 weeks, there was no obvious change of current. After the sensor was stored in an inverted beaker at 4°C for 60 days the current response to 0.5 mM NO_2^- only decreased by 7.8% from the original value. The current response kept 95% of the original current for 0.5 mM NO_2^- in 30 min, indicating that the maximum time that the sensor could be operated in one measurement without significant deterioration was about 30 min.

Conclusion

In this work, the $PW_{12}O_{40}^{3-}$ and CHIT-graphene nanocomposites were introduced to construct a NO_2^- sensor. The sensor has the advantages of quick amperometric response, low detection limit, wide linear range, high sensitivity, high stability, and good reproductively as compared with previous results. The good electrocatalytic performance can be ascribed to large surface area, good conductivity of the CHIT-graphene nanocomposites, and good catalytic activity of $PW_{12}O_{40}^{3-}$. The good analytical performance suggested that it is possible to be a potential candidate for routine NO_2^- analysis.

Acknowledgments

This work was financially supported by National Natural Science Foundation of China (21065005, 51165010, and 21101146), Young Scientist Foundation of Jiangxi Province (20112BCB23006 and 20122BCB23011), Foundation of Jiangxi Educational Committee (GJJ13243 and GJJ13244), and the Open Project Program of Key Laboratory of Functional Small Organic Molecule, Ministry of Education, Jiangxi Normal University (No. KLFS-KF-201214 and KLFS-KF-201218).

Author Disclosure Statement

No competing financial interests exist.

References

Bertotti, M., and Pletcher, D. (1997). Amperometric determination of nitrite via reaction with iodide using microelectrodes. *Anal. Chim. Acta* 337, 49.

Cao, F., Guo, S., Ma, H., and Gong, J. (2012). ITO electrode modified by α-$K_6[P_2W_{18}O_{62}]$ hybrid nanofibers for nitrite determination. *Electroanalysis* 24, 418.

Castillo, M.A., and Castells, R.C. (2001). Initial evaluation of quantitative performance of chromatographic methods using replicates at multiple concentrations. *J. Chromatogr. A* 921, 121.

Chen, C., Song, Y., and Wang, L. (2008). A novel sensor based on layer-by-layer hybridized phosphomolybdate and poly(-ferrocenylsilane) on a cysteamine modified gold electrode. *Electroanalysis* 20, 2543.

Chen, C., Song, Y., and Wang, L. (2009). Electrochemical behavior and its electrocatalytic properties of chemically modified electrode with Keggin-type $[SiNi(H_2O)W_{11}O_{39}]^{6-}$. *Electrochim. Acta* 54, 1607.

Cui, L., Pu, T., Liu, Y., and He, X. (2013). Layer-by-layer construction of graphene/cobalt phthalocyanine composite

film on activated GCE for application as a nitrite sensor. *Electrochim. Acta* 88, 559.

Gu, Y., Ma, H., O'Halloran, K.P., Shi, S., Zhang, Z., and Wang, X. (2009). An α-$K_3PMo_3W_9O_{40}$ film loaded with silver nanoparticles: Fabrication, characterization and properties. *Electrochim. Acta* 54, 7194.

Hamidi, H., Shams, E., Yadollahi, B., and Esfahani, F.K. (2008). Fabrication of bulk-modified carbon paste electrode containing α-$PW_{12}O_{40}^{3-}$ polyanion supported on modified silica gel: Preparation, electrochemistry and electrocatalysis. *Talanta* 74, 909.

Han, D., Han, T., Shan, C., Ivaska, A., and Niu, L. (2010). Simultaneous determination of ascorbic acid, dopamine and uric acid with chitosan-graphene modified electrode. *Electroanalysis* 22, 2001.

Hummers, W.S., and Offeman, R.E. (1958). Preparation of graphitic oxide. *J. Am. Chem. Soc*. 80, 1339.

Laviron, E. (1979). General expression of the linear potential sweep voltammogram in the case of diffusionless electrochemical systems. *J. Electroanal. Chem. Interfacial Electrochem.* 101, 19.

Li, C., Zhang, Y., O'Halloran, K.P., Zhang, J., and Ma, H. (2008). Electrochemical behavior of vanadium-substituted Keggin-type polyoxometalates in aqueous solution. *J. Appl. Electrochem.* 39, 421.

Liu, K., Zhang, J., Yang, G., Wang, C., and Zhu, J.-J. (2010). Direct electrochemistry and electrocatalysis of hemoglobin based on poly(diallyldimethylammonium chloride) functionalized graphene sheets/room temperature ionic liquid composite film. *Electrochem. Commun.* 12, 402.

Liu, Y., and Gu, H.-Y. (2008). Amperometric detection of nitrite using a nanometer-sized gold colloid modified pretreated glassy carbon electrode. *Microchim. Acta* 162, 101.

Mani, V., Periasamy, A.P., and Chen, S.-M. (2012). Highly selective amperometric nitrite sensor based on chemically reduced graphene oxide modified electrode. *Electrochem. Commun.* 17, 75.

Molina, J., del Río, A.I., Bonastre, J., and Cases, F. (2008). Chemical and electrochemical polymerisation of pyrrole on polyester textiles in presence of phosphotungstic acid. *Eur. Polym. J.* 44, 2087.

Ojani, R., Rahmanifar, M.S., and Naderia, P. (2008). Electrocatalytic reduction of nitrite by phosphotungstic heteropolyanion. Application for its simple and selective determination. *Electroanalysis* 10, 1092.

Rahman, M.A., Won, M.-S., Wei, P.-H., and Shim, Y.-B. (2006). Electrochemical detection of ClO, BrO, and IO at a phosphomolybdic acid linked 3-aminopropyl-trimethoxysilane modified electrode. *Electroanalysis* 18, 993.

Stankovich, S., Dikin, D.A., Piner, R.D., Kohlhaas, K.A., Kleinhammes, A., Jia, Y., Wu, Y., Nguyen, S.T., and Ruoff, R.S. (2007). Synthesis of graphene-based nanosheets via chemical reduction of exfoliated graphite oxide. *Carbon* 45, 1558.

Unnikrishnan, B., Ru, P.-L., Chen, S.-M., and Mani, V. (2013). Nitrite determination at electrochemically synthesized polydiphenylamine-Pt composite modified glassy carbon electrode. *Sens. Actuators B Chem.* 177, 887.

Wang, D., Kou, R., Choi, D., Yang, Z., Nie, Z., Li, J., Saraf, L.V., Hu, D., Zhang, J., Graff, G.L., *et al*. (2010). Ternary self-assembly of ordered metal oxide-graphene nanocomposites for electrochemical energy storage. *ACS Nano* 4, 1587.

Wang, L., Zhu, H., Song, Y., Liu, L., He, Z., Wan, L., Chen, S., Xiang, Y., Chen, S., and Chen, J. (2012). Architecture of poly(o-phenylenediamine)–Ag nanoparticle composites for a hydrogen peroxide sensor. *Electrochim. Acta* 60, 314.

Xu, J., Shang, F., Luong, J.H., Razeeb, K.M., and Glennon, J.D. (2010). Direct electrochemistry of horseradish peroxidase immobilized on a monolayer modified nanowire array electrode. *Biosens. Bioelectron.* 25, 1313.

Yang, X., Tu, Y., Li, L., Shang, S., and Tao, X.M. (2010). Well-dispersed chitosan/graphene oxide nanocomposites. *ACS Appl. Mater. Interfaces* 2, 1707.

Zhu, S.H., Gao, X.Q., Dong, F., Zhu, Y.L., Zheng, H.Y., and Li, Y.W. (2013). Design of a highly active silver-exchanged phosphotungstic acid catalyst for glycerol esterification with acetic acid. *J. Catal*. 306, 155.

This article has been cited by:

1. Zhenyuan Bai, Chunlei Zhou, Ning Gao, Haijun Pang, Huiyuan Ma. 2016. A chitosan–Pt nanoparticles/carbon nanotubes-doped phosphomolybdate nanocomposite as a platform for the sensitive detection of nitrite in tap water. *RSC Adv.* **6**, 937-946. [CrossRef]